International Journal of Heat and Fluid Flow 32 (2011) 1138–1146

Contents lists available at SciVerse ScienceDirect

International Journal of Heat and Fluid Flow

journal homepage: www.elsevier.com/locate/ijhff

Comparison of flow structures in the downstream region of a cylinder and sphere

Muammer Ozgoren [a], Engin Pinar [b], Besir Sahin [b,*], Huseyin Akilli [b]

[a] Selçuk University, Faculty of Engineering and Architecture, Department of Mechanical Engineering, Konya, Turkey
[b] Çukurova University, Faculty of Engineering and Architecture, Department of Mechanical Engineering, Adana, Turkey

ARTICLE INFO

Article history:
Received 16 November 2009
Received in revised form 14 August 2011
Accepted 31 August 2011
Available online 25 September 2011

Keywords:
Cylinder
PIV
Sphere
Vorticity
Vortex shedding
Wake flow

ABSTRACT

An experimental investigation of flow structures downstream of a circular cylinder and sphere immersed in a free-stream flow is performed for Re = 5000 and 10,000 using qualitative and quantitative flow visualization techniques. The obtained results are presented in terms of time-averaged velocity vectors, patterns of streamlines, vorticity, Reynolds stress correlations and turbulent kinetic energy distributions. Flow data reveal that the size of wake flow region, the location of singular and double points, the peak values of turbulence quantities, such as Reynolds stress correlations, vorticity fluctuations and turbulent kinetic energy vary as a function of models' geometry and Reynolds Numbers. The concentration of small scale vortices is more dominant in the wake of the sphere than that of the cylinder. The maximum value of turbulent kinetic energy (TKE) occurs close to the saddle point for the cylinder case while two maximum values of TKE occur along shear layers for the sphere one because of the 3-D flow behavior.

1. Introduction

Flow past a bluff body such as a sphere and cylinder from engineering application point of view is a generic flow–structure interaction with important implications for flow-induced vibration and noise generation. Periodic vortex shedding patterns and fluctuating velocity fields downstream of the bluff bodies can cause structural damage because of periodic surface loading, acoustic noise and drag forces. Most work has been done on the flow passing a circular cylinder rather than a sphere.

Relevant investigations for the cylinder include those of Sahin and Ozturk (2009), Sahin et al. (2007), Ozgoren (2006), Akilli et al. (2004), Noca et al. (1998), Balachandar et al. (1997), Lin et al. (1995) and Bloor and Gerrard (1966) using various measurement techniques. More detailed results for flow characteristics around circular cylinder wakes and vortex-induced vibrations were given with review studies of Bearman (2011), Williamson and Govardhan (2004), Sarpkaya (2004), Norberg (2003), Williamson (1996), Parkinson (1974) and cited therein. Sahin et al. (2007) concentrated on the flow structure around the base of a vertical cylinder mounted on a flat plate with a Reynolds number of Re = 4000 using the PIV technique. They pointed out that the structure of turbulent flow, the size of the wake flow region, the location of singular points, the peak values of turbulent quantities such as Reynolds stress correlations, $\langle u'v'/U_\infty^2 \rangle$, and the root mean square of the velocity components, $\langle u_{rms}/U_\infty \rangle$ and $\langle v_{rms}/U_\infty \rangle$, vary as a function of elevation of the laser sheet location in the region of the boundary layer. Ozgoren (2006) examined the flow characteristics downstream of a single circular, a sharp-edged square and a 45° orientated square cylinder in a uniform flow in the range of $550 \leqslant Re \leqslant 3400$ using PIV. Noca et al. (1998) accomplished an investigation on the concept of vortex formation length in the wake of the cylinder for $300 \leqslant Re \leqslant 4000$ and different aspect ratios. Balachandar et al. (1997) applied direct numerical simulations at lower Reynolds numbers and large-eddy simulation at higher Reynolds numbers over several different 2D bluff bodies for $250 \leqslant Re \leqslant 140{,}000$. The work of Zdravkovich (1997) reported a detailed flow field description around circular cylinders. Williamson (1996) gives a comprehensive review on vortex dynamics in the wake of a circular cylinder. Three-dimensional vortex patterns in the laminar vortex shedding regime and three-dimensional vortex dynamics in the transition regime were discussed. Flow structures around cylinders were investigated quantitatively by Lin et al. (1995) for Re = 1000, 5000 and 10,000. They stated that velocity distributions, patterns of streamlines and vorticity indicated a decrease in vortex formation length with increasing Reynolds number. Furthermore, a crucial phenomenon occurring Reynolds number range of 3900–20000 is the onset and the amplification of the Kelvin–Helmholtz (KH) instability in the free shear layer formed from the surface of cylinder, producing small-scale vortices ad recorded by Bloor and Gerrard (1966), Gerrard (1965) and Rajagopalan and Antonia, 2005). The numerical and modeling aspects are investigated by Breuer (1998, 2000), who employs five different numerical schemes and two subgrid-scale models in LES. It is recorded that the predicted integral parameters

* Corresponding author. Tel.: +90 322 3387063; fax: +90 322 3386126.
E-mail addresses: mozgoren@selcuk.edu.tr (M. Ozgoren), en_pinar@hotmail.com (E. Pinar), bsahin@cu.edu.tr (B. Sahin), hakilli@cu.edu.tr (H. Akilli).

0142-727X/$ - see front matter © 2011 Elsevier Inc. All rights reserved.
doi:10.1016/j.ijheatfluidflow.2011.08.003

and the mean velocity profiles are in reasonable agreement with the experimental data.

In particular the sphere is regarded as a representative three-dimensional bluff body, and its wake structure is quite complex because of 3-D vortex shedding (Achenbach, 1974; Constantinescu and Squires, 2003; Johnson and Patel, 1999; Kim and Durbin, 1988; Mittal, 1999; Mittal and Najjar, 1999; Leder and Geropp,1993; Sakamoto and Haniu, 1990; Taneda, 1978; Hadzic et al. (2002);Yun et al., 2006; Jeon and Choi, 2010). The flow around a sphere shows steady and axi-symmetric flow for $20 \leqslant Re \leqslant 210$. The axi-symmetric flow is then broken, and planar-symmetric flow appears until Re = 280. From Re = 280, unsteadiness starts to occur in the planar-symmetric flow, and hairpin vortices are periodically shed. In the range of Reynolds numbers $420 \leqslant Re \leqslant 800$, asymmetric flow is observed, and unsteadiness continues as reported by Leweke et al., 1999; Wu and Faeth, 1993; Johnson and Patel, 1999; Nakamura, 1976 and Taneda, 1978. On the other hand, the large-scale low-frequency vortex shedding and small-scale high-frequency shear layer instabilities dominate the flow field when $Re \geqslant 800$. In addition, a large-scale vortex is shed with wavy shape, and turbulence occurs in the far field. At the critical Reynolds number of $Re = 3.7 \times 10^5$, the drag coefficient is rapidly reduced. In the subcritical Reynolds numbers in the range of $800 \leqslant Re \leqslant 3.7 \times 10^5$, the drag coefficient of a sphere has almost constant values with laminar boundary layer. Furthermore, Kelvin–Helmholtz instability occurs in the separating shear layers causing high rate of turbulence in the wake region. A few experimental studies on the turbulent flow around a sphere have been conducted in the subcritical Reynolds number regime. Jang and Lee (2008) reported the vortical flow structures of the sphere wake in the streamwise plane at Re = 11000 in order to demonstrate flow structures and turbulence statistics. Their results could enhance understanding of the vortical flow structure and shear-layer instability inside the near-wake of a sphere.

Ozgoren et al. (2006) have reported useful information about flow structure around a single spherical body as a preliminary study. Kiya et al. (2001) and Sakamoto and Haniu (1990) classified sphere wake patterns according to Strouhal number for $300 \leqslant Re \leqslant 4 \times 10^4$. They observed vortex-tube pulsations and periodic vortex shedding incorporating asymmetric flow, as well as an irregularly rotating separation angle, a cylindrical-shaped shear layer instability and irregular shedding with wavy progress of the wake. Kim and Durbin (1988) found two frequency modes in the turbulent wake downstream of a sphere which are related to the small-scale instability of the separating shear layers and to the large scale instability of the wake. Werle (1980) visualized sphere wakes in a water tunnel using dye at $Re = 1.6 \times 10^4$ in order to see the recirculating flow downstream of a sphere and the shear layer instability of a ring-shaped vortex. Achenbach (1972, 1974) visualized the vortical structure of sphere wake at Re = 1000 using a dye method and measured skin friction to investigate flow-separation angles in the range of $10^5 \leqslant Re \leqslant 10^6$.

The motivation for this research can be explained as follows. Most previous experimental works on cylinder and sphere wakes have been carried out using point-wise measurement methods and conventional flow visualization techniques. Recently, many numerical simulations have been conducted to investigate cylinder and sphere wakes with improved turbulence models. However, the numerical simulations have a difficulty in validating their predicted results with comparative experimental data. The purpose of this study is to investigate and compare the flow patterns of the sphere and cylinder with a global visualization technique of PIV and dye experiments in the moderate Reynolds number range. This visualization will be supported by spectra of the near-wake velocity fluctuations, which provide an additional and complementary means of determining vortex shedding frequency.

2. Experimental setup

Experiments were performed in a large-scale open water channel with a test section length of 8000 mm and a width of 1000 mm at the Department of Mechanical Engineering at Cukurova University, Turkey. To perform the present experimental study, the test section made from 15 mm thick transparent Plexiglas sheet, which had a total height of 750 mm, was filled with water to a level of only 450 mm. Before reaching the test chamber, the water was pumped into a settling chamber and passed through a honeycomb section and a two-to-one channel contraction. An overview of experimental system of the sphere and the cylinder is shown in Fig. 1. Free stream turbulence intensity of the flow is less than 0.5% in the range of the present Reynolds numbers, $Re = (U_\infty D)/\nu$, based on the bluff body diameter (D). Here, ν and D are kinematics viscosity and diameter of the cylinder (D_c) or sphere (D_s), respectively. U_∞ is free-stream velocity ranging from 50 to 235 mm/s. The cylinder with a diameter of 50 mm and the sphere with a diameter of 42.5 mm made of Plexiglas were used. The sphere is hollow and filled with water in order to reduce largely the laser light deflection on the sphere. The surface of the sphere was polished to avoid effects of surface roughness.

The laser sheet was located at 225 mm above the bottom surface of the channel while the water height h_w was 450 mm in all cases. Free-surface of the water flow did not affect the flow in the measurement plane since the Froude Number of the water channel flow was well below than the critical Froude number for Re = 5000 and 10000 which were respectively $Fr = U_\infty/\sqrt{gh_w} = 0.056$ and 0.112. To support the sphere in the water channel, a circular bar with a 5 mm diameter was connected to the sphere from the top. Disturbance effect of the support bar on the flow structure for both horizontal and cross-section planes was negligible that was observed by dye visualization.

Nd:YAG laser was used to generate a laser sheet that was passed perpendicularly to the axis of the cylinder and the symmetry axis (i.e. equator) of the sphere. A CCD camera having a resolution of 1600×1186 pixels was used to record the images. The seeding particles with a diameter of 10 μm in the flow were silver metallic coated, hollow plastic spheres. The densities of the particles and water are close enough so that the distribution of particles in suspension remains uniform for several hours. As shown in Fig. 1, the camera was mounted in a fixed position beneath the water tank. Dantec Flow Grabber digital PIV software employing the cross-correlation algorithm was used to compute the raw displacement vector field from the particle image data. An interrogation window of 32×32 pixels in the image was selected and converted to grid size approximately $2.2 \times 2.2\ mm^2$ for the cylinder and $1.5 \times 1.5\ mm^2$ for the sphere. The overall fields of physical view were $211.9 \times 155.7\ mm^2$ for the cylinder and $145.8 \times 107.2\ mm^2$ for the sphere, yielding to 7227 (99×73) velocity vectors. During the interrogation process, an overlap of 50% was employed in order to satisfy

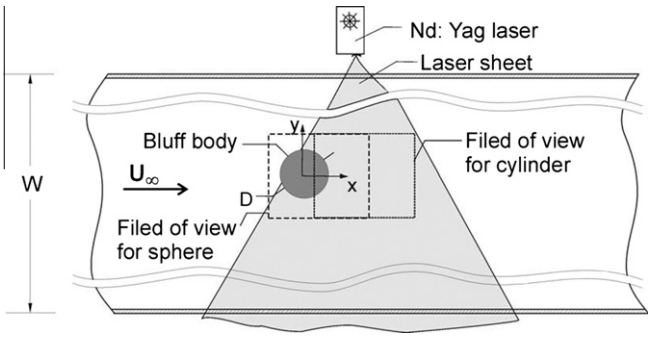

Fig. 1. Schematic of the experimental system and definition of the parameters for the two models.

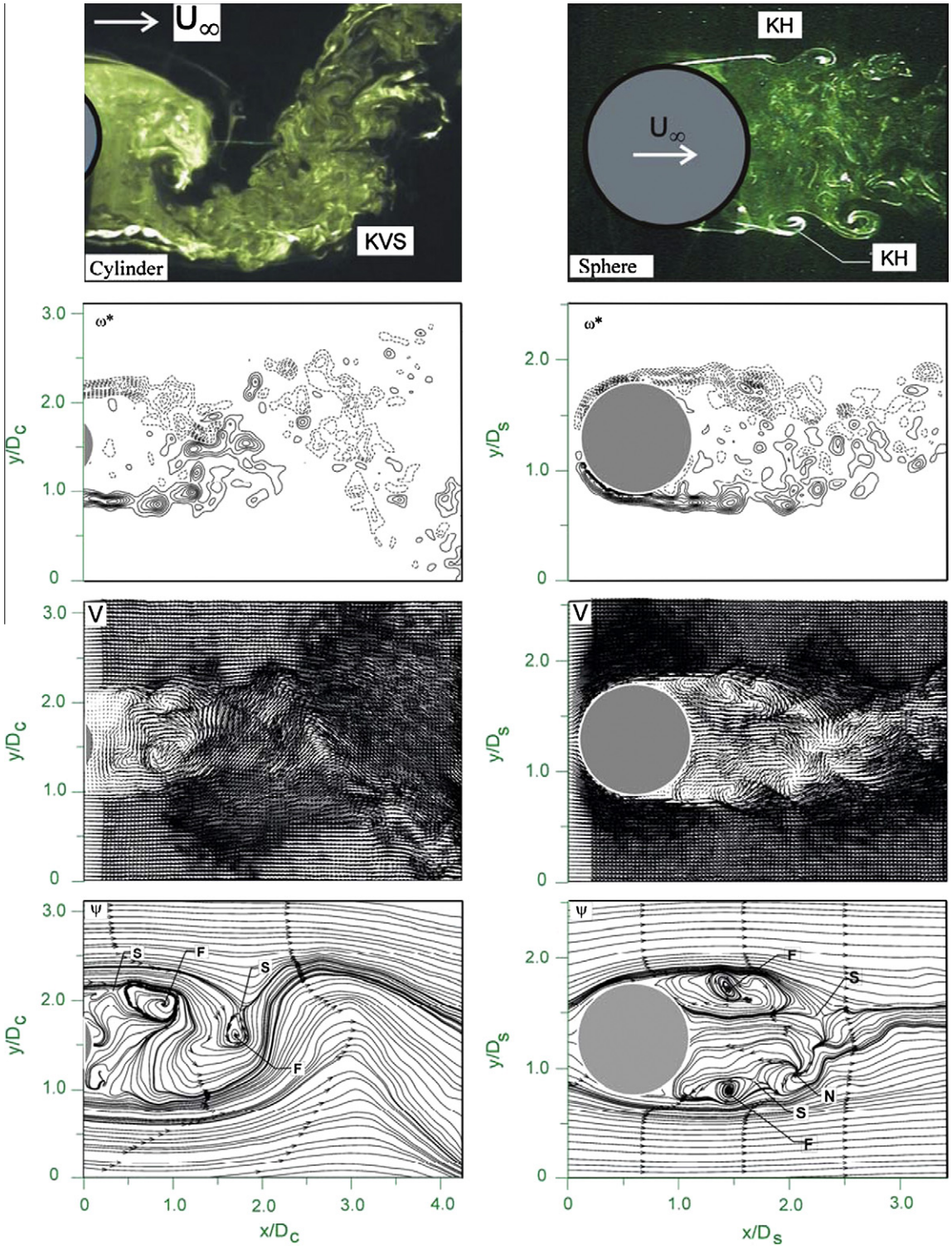

Fig. 2. Comparison of dye visualization and instantaneous vorticity ω^*, velocity field V and instantaneous streamline patterns ψ for the two models at Re = 5000. Minimum and incremental values of instantaneous vorticity ω^* are both 2.

the Nyquist criterion. Patterns of instantaneous particle images with a total of 350 images for a continuous series were taken at the rate of 15 Hz, The laser sheet was generated from a dual pulsed Nd:YAG system, having the maximum output of 120 mJ per pulse, which had time delays ranging from Δt = 1.7 ms to 4.5 ms. Inappropriate displacement vectors caused by shadows, reflections, or laser sheet distortions in the flow field replaced by using bilinear interpolation between surrounding vectors in the post-processing step. The field was then smoothed by a Gaussian weighted averaging technique. To minimize distortion of the velocity field, a smoothing parameter

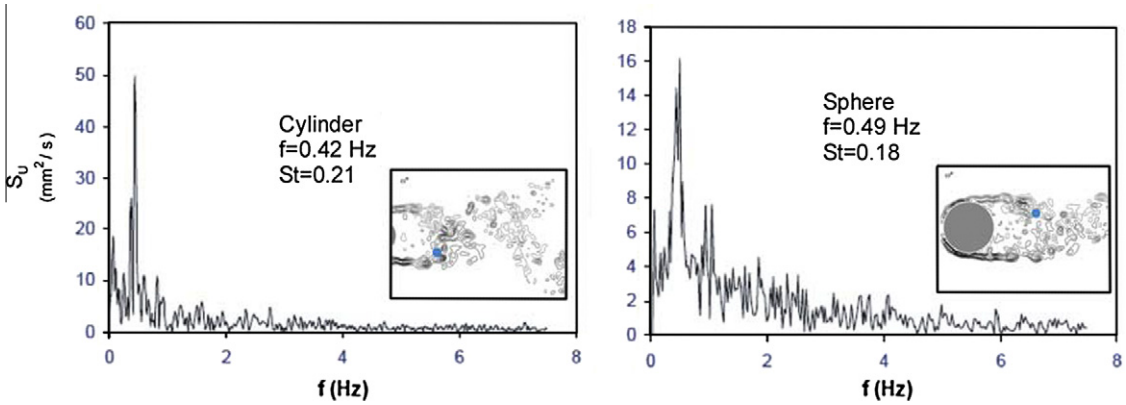

Fig. 3. Comparison of FFT result variations f (Hz) against spectral density S_u (mm^2 s) at denoted point with small circle for the two models at Re = 5000, which is derived from time history of instantaneous streamwise velocity component u (mms).

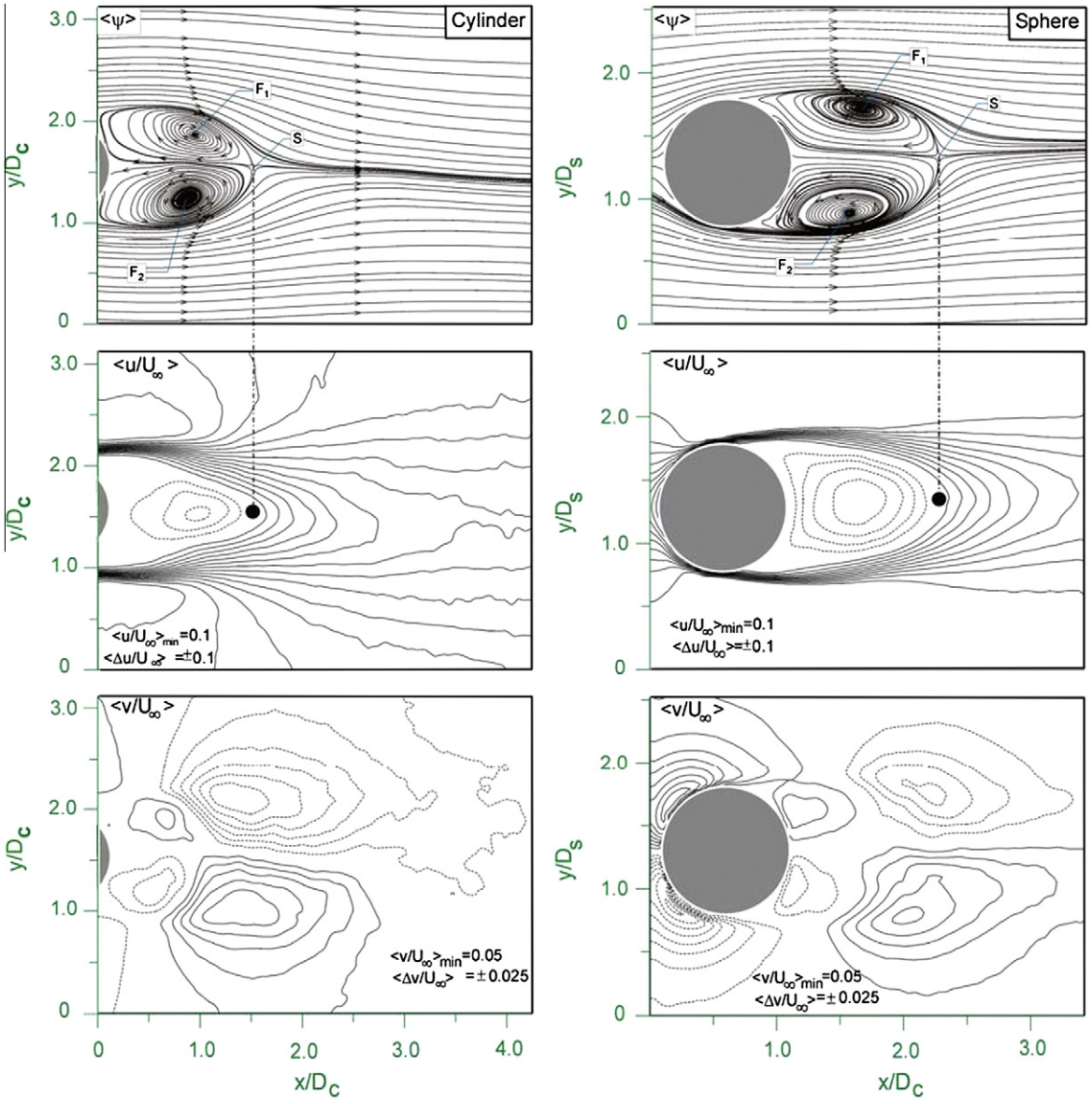

Fig. 4. Comparison of flow patterns of the cylinder (left column) and sphere (right column) for streamline topology $\langle\psi\rangle$ streamwise velocity component $\langle u/U_\infty\rangle$ and cross-stream velocity component $\langle v/U_\infty\rangle$ for Re = 5000.

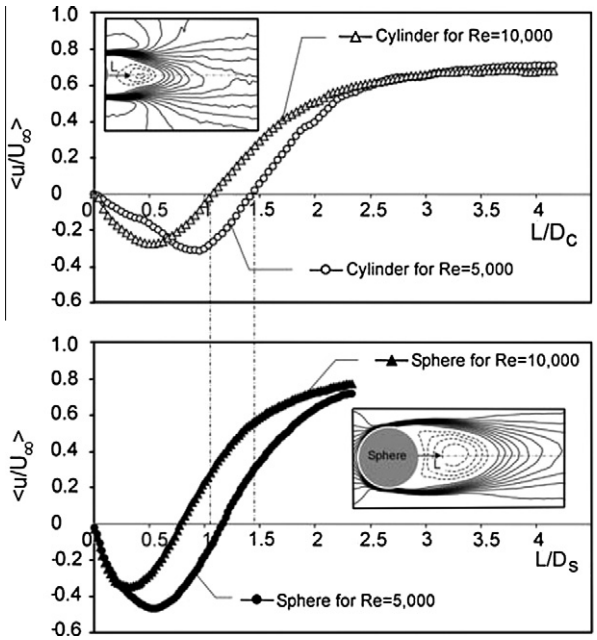

Fig. 5. Variation of time-averaged streamwise velocity component $\langle u/U_\infty \rangle$ along the centerline axis of the cylinder and sphere for Re = 5000 and Re = 10,000.

of 1.3 was chosen. After having been vector field, the vorticity patterns of the wake flow were determined from the velocity field using a second order finite difference scheme.

The factors contributing to uncertainty in the velocity measurement using the PIV technique were critically assessed by Westerweel (1993) who concluded that uncertainty estimation in the velocity measurement was less than 2%.

3. Results and discussion

3.1. Flow visualization and instantaneous flow patterns

Fig. 2 shows qualitative and quantitative flow visualization images of instantaneous flow fields around a cylinder and sphere model at Re = 5000. The separated and recirculating flow in the near-wake region is clearly visualized with laser illumination using Rhodamine dye injection. Small scale vortices around the wake region are formed to create large-scale vortices with a wavy appearance due to Kelvin Helmholtz (KH) instability. The formation of vortices begins to occur in the region very close to the sphere. As the flow travels downstream, the size of vortices increase. Then these vortices are shed from the periphery of the sphere directly into inner wake region. Kármán vortex streets (KVS) form a little further downstream shown in Fig. 2. By comparison, in the case of the cylinder, the well-known Kármán vortex occurs immediately caused by the flow separation as demonstrated in Fig. 2. The large eddies are formed at a regular frequency, and they produce pressure disturbances in the flow. As seen from the top image in Fig. 2, a dominant large-scale Kármán vortex occurs in the lower side of the cylinder. Laminar boundary layer flow separation is developed near the equator of the sphere model, while it is recorded around 82° from the front stagnation point of the cylinder. The circulating flow region formed downstream of the sphere is visualized, which is convected upstream by a reverse flow and downstream by a momentum transfer. The laminar shear layer becomes unstable approximately one diameter further downstream from the sphere due to the Kelvin–Helmholtz (KH) instability caused by the large velocity differences at the interface between the free-stream and sphere wake flow regions. Later, the laminar shear layer turns into a turbulent flow structure. Several vortex-ring shaped protrusions appear as an indication of the shear-layer instability along the borders between the wake and free-stream regions, as stated by Jang and Lee (2008).

Representative instantaneous vorticity contours ω of the wake structure for the cylinder and sphere geometries at Re = 5000, normalized as $\omega^* = \omega D/U$ are illustrated in the second row of Fig. 2. All images are normalized with the cylinder and sphere diameters designated as x/D_c, y/D_c, x/D_s and y/D_s. Viewing the Von Karman vortex street in the horizontal plane, concentrated vorticity layers are shed into downstream flow from alternate sides of the body, creating of an upper row of negative vortices (dashed lines) and a lower row of positive vortices (solid lines). The cylinder wake region is wider than the sphere wake region because of having 2D flow and the earlier occurrence of the KVS. The vortices produced from the flow separation around the periphery of the sphere have a tendency to move inwards because of the pressure differences between the main and wake flow regions. This situation is counter-balanced by the growing wake size. The small-scale vortical structures in the separating shear layer regions are observed in the pattern of instantaneous vorticity for the two models. Large-scale Kármán vortices form in the near-wake region due to the abrupt coalescence of small-scale vortices that developed along the separating shear layers, as obtained by Lin et al. (1995) and Ozgoren (2006). Instantaneous vorticity patterns show irregular vorticity distributions, and the shear layers tend to break up easily into small concentrations of vorticity related to Kelvin–Helmholtz (KH) instabilities for the two models. Concentrations of the small-scale vortices for the sphere are stronger than those for the cylinder case. Vortices in the upper and lower regions of the symmetry axis look similar in size and shape to the sphere case. Comparison of instantaneous velocity fields for the two models is displayed in the third row of Fig. 2. All of the images in the left column for the cylinder show the existence of Von Karman vortex streets, clearly. The separated flow rotates in the clockwise direction in the downstream region of the cylinder, while it becomes nearly symmetric in the case of the sphere. Approximately $1.0D_s$ or $1.5D_s$ downstream of the sphere base, flow symmetry is degraded, and Karman vortex streets begin to appear. The wake region accommodates velocity vectors with very small magnitude in the downstream region of the two models, which are the source of small-scale secondary vortices, as seen in the second row of Fig. 2. The streamwise separation of successive vorticity peaks in the near wake region for the cylinder is larger than that for the sphere. The shedding vortices convey fresh fluid into the wake flow region and thus magnifying the entrainment.

Comparison of corresponding instantaneous streamline patterns for the two models at Re = 5000 is shown in the last row of Fig. 2. Patterns of streamlines are developed with an *S*-shape downstream of the cylinder demonstrating well defined KVS. Streamline patterns in Fig. 2 have a high rate of unsteadiness and complex flow structures, which generates multi saddle points (*S*) and focus (*F*) in the cases of both models. For the sphere, shear layers emanating from the sphere circumference merge at a location at nearly $1.0D_s$ and later generate KVS. The domains of focus for the sphere are wider than those for the cylinder due to the 3-D flow characteristics.

3.2. Spectral analysis and calculation of vortex shedding frequency

It is seen that well known Karman vortex streets are formed in the cylinder wake region, whereas shedding vortices are attached circumferentially on the sphere surface. The oscillating wake rolls up into two staggered rows of vortices with opposite senses of rotation. The frequency of vorticity pairs is a function of velocity,

bluff body diameter and Reynolds number, as stated by Williamson (1996). The dominant vortex shedding frequency, f is determined from power spectra of the recorded PIV data in the near wake regions of the two models, at selected points located in the inner regions of the shear layers. FFT analysis reveals vortex shedding frequency, as seen in Fig. 3, the peak frequencies of vortex shedding are calculated as 0.42 Hz and 0.49 Hz for the cylinder and the sphere, respectively. Corresponding Strouhal numbers, $St = fD/U_\infty$ for the cylinder and the sphere are found to be 0.21 and 0.18, respectively. Strouhal numbers are obtained in the range of $0.18 \leqslant St \leqslant 0.24$ for Reynolds numbers of $2500 \leqslant Re \leqslant 10{,}000$ in various points of the wake region of the sphere. The value of the St number results agrees well with the results of Jang and Lee (2008), Suryanarayana and Prabhu (2000) and Sakamoto and Haniu (1990). Strouhal numbers obtained for the cylinder almost match the value of 0.21, which agrees with the results of King (1977),

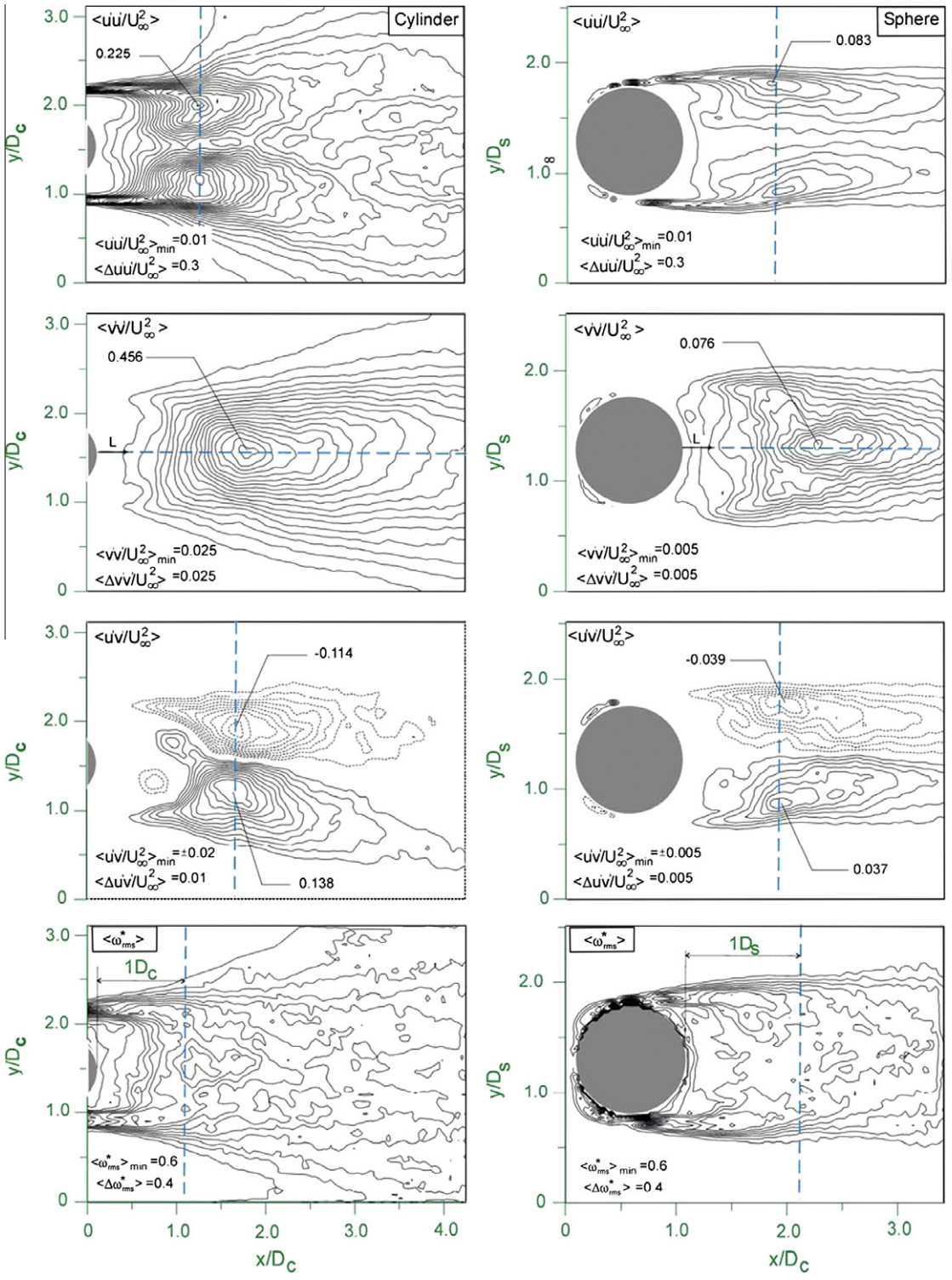

Fig. 6. Comparison of normalized time-averaged flow patterns of streamwise Reynolds normal stress $\langle u'u'/U_\infty^2 \rangle$, transverse Reynolds normal stress $\langle v'v'/U_\infty^2 \rangle$, Reynolds stress correlations $\langle u'v'/U_\infty^2 \rangle$ and vorticity fluctuations $\langle \omega^*_{rms} \rangle$ at Re = 5000.

Akilli et al. (2004) and Ozgoren (2006) who found Strouhal number for the cylinder as St ≈ 0.21 over a wide range of Reynolds numbers, for example, $10^2 \leqslant Re \leqslant 10^5$.

3.3. Time-averaged flow patterns

Comparison of the normalized flow patterns of the cylinder and the sphere, time-averaged streamline patterns $\langle\psi\rangle$, streamwise velocity component $\langle u/U_\infty\rangle$, cross-stream velocity component $\langle v/U_\infty\rangle$, streamwise Reynolds normal stress $\langle u'u'/U_\infty^2\rangle$, transverse Reynolds normal stress $\langle v'v'/U_\infty^2\rangle$, Reynolds stress correlations $\langle u'v'/U_\infty^2\rangle$, rms (root mean square) contours of vorticity $\langle\omega^*_{rms}\rangle$ ($\langle\omega^*_{rms}\rangle$=$\omega^*_{rms}$D/$U_\infty\rangle$) are displayed in Figs. 4–7. For these and other figures, the minimum and normalized incremental values of the patterns are given on each image.

As seen in the top row of Fig 4., the time-averaged streamline topology is interpreted in terms of foci, *F*, and saddle points, *S*. Comparison of the time-averaged patterns shows that flow structures of the wake are almost equally symmetrical with respect to centerlines of the two models. Patterns of time-averaged streamline topology $\langle\psi\rangle$ identify the major changes of the near-wake downstream of the cylinder. They exhibit well-defined critical points, foci, F_1 and F_2 and saddle points *S*. The saddle point indicated by the time-averaged streamline topology is developed earlier for the sphere than the cylinder. These well defined large-scale vortices occupying whole wake regions agree well with the previous studies of Jang and Lee (2008) and Ozgoren et al.(2006). The non-dimensional wake lengths (*L*/*D*) measured from the rear surface of the two models to the saddle points *S* are approximately $1.50D_c$ and $1.15D_s$ for Re = 5000. Representations of the streamwise velocity component $\langle u/U_\infty\rangle$ over the entire field of view given in the second row of Fig. 4 also presents the location of the stagnation point along the plane of wake symmetry as indicated by a black dot. The distances between the rear surface of the cylinder or

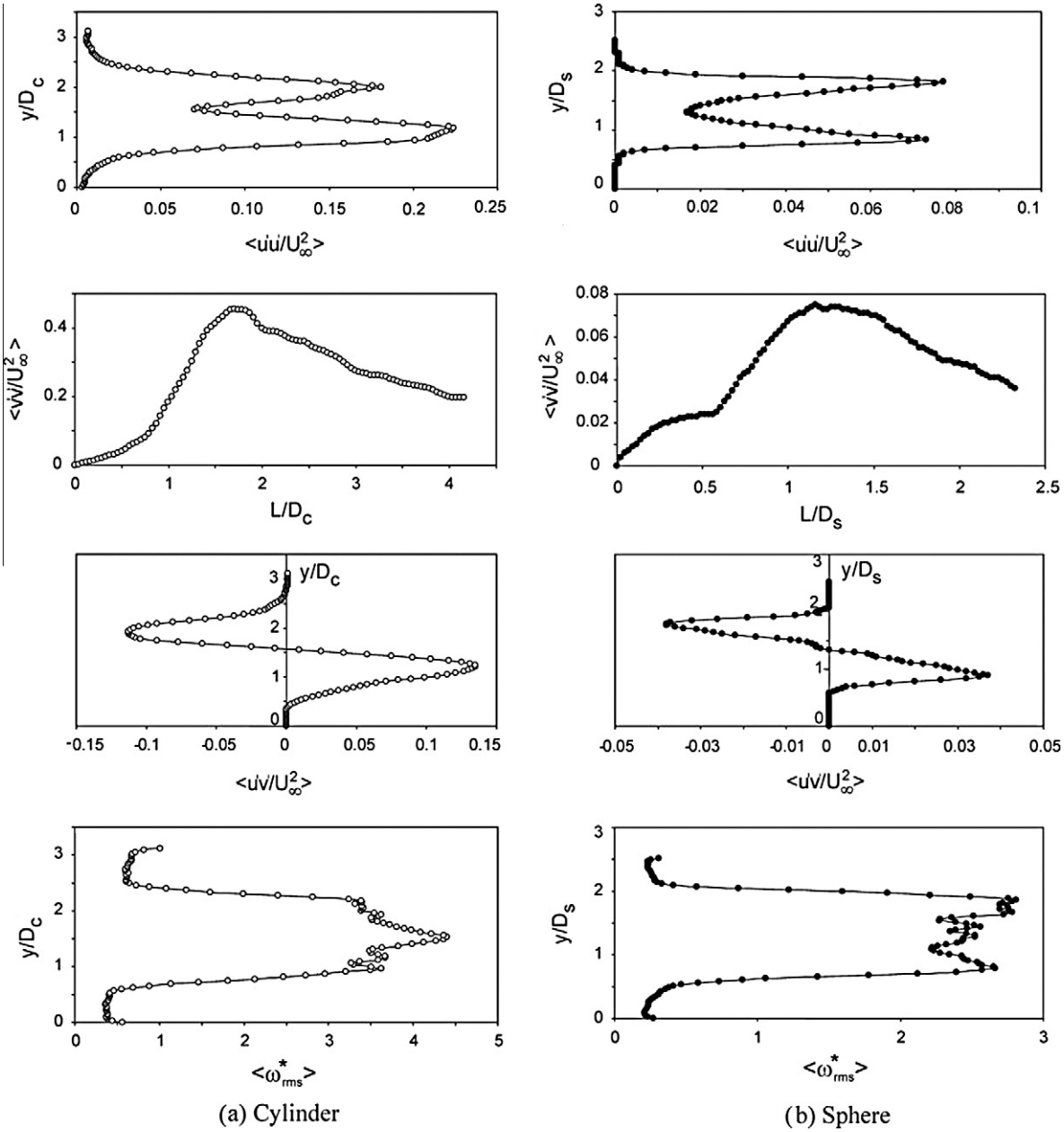

Fig. 7. Comparison of normalized time-averaged flow data along vertical or horizontal dashed lines, indicated in Fig. 6, in the downstream of the cylinder with the symbol "-○- and sphere with the symbol "-●-" for Re = 5000.

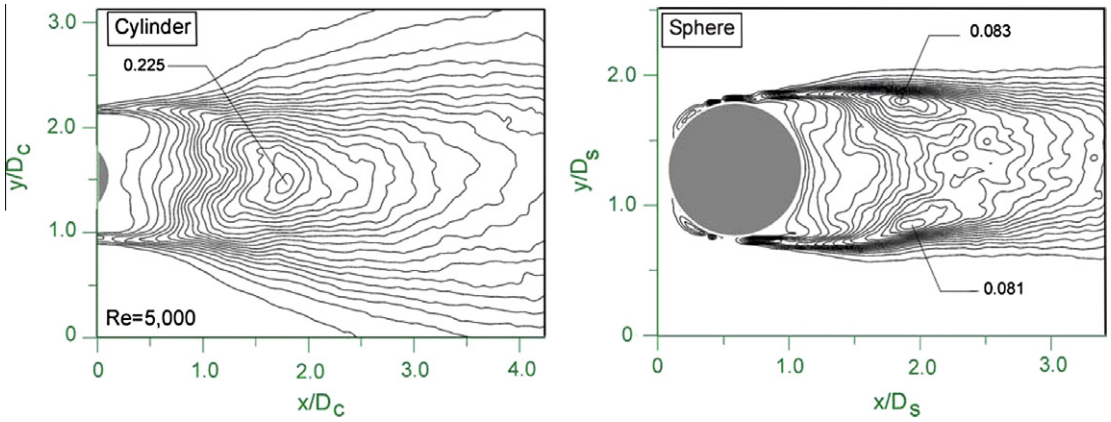

Fig. 8. Comparison of normalized TKE distribution in the downstream of the two models for Re = 5000. Minimum and incremental contour values of TKE for the cylinder and the sphere are 0.02 and 0.005, respectively.

sphere and the stagnation point are approximately $1.47D_c$ and $1.15D_s$, respectively. Two different pairs of clusters of time-averaged cross-stream velocity component $\langle v/U_\infty \rangle$ presented at the bottom row of Fig. 4 were developed downstream of both models. Contours of cross-stream velocity components, $\langle v/U_\infty \rangle$ are involved in a "switching" of the orientation of the positive and negative values of $\langle v/U_\infty \rangle$ downstream of the two models. Variations of the time-averaged streamwise velocity component $\langle u/U_\infty \rangle$ along the centerline axis of the two models for Re = 5000 and Re = 10,000 are shown in Fig. 5. The vortex formation lengths for the two models are overlapped as indicated in Fig. 4 and 5. As the Reynolds number is increased to a value of Re = 10,000, these vortices are developed in a shorter distance and are placed close to the bluff body.The vortex formation length in the wake region of the two models can also be described by means of the point of maximum values of streamwise Reynolds normal stress $\langle u'u'/U_\infty^2 \rangle$, transverse Reynolds normal stress $\langle v'v'/U_\infty^2 \rangle$ and Reynolds shear stress correlations $\langle u'v'/U_\infty^2 \rangle$. As seen in Fig. 6, the maximum values of the streamwise Reynolds normal stress $\langle u'u'/U_\infty^2 \rangle$ with double peaks for the two models occur at locations of approximately $0.85D_s$ and $1.17D_c$ whereas those of transverse Reynolds normal stress $\langle v'v'/U_\infty^2 \rangle$ with a single peak is placed at locations of approximately $1.16D_s$ and $1.72D_c$.

Reynolds stress correlations $\langle u'v'/U_\infty^2 \rangle$ depict a set of extrema on either side of the wake centerline for the cylinder and sphere in the third row of Fig. 6. The patterns of the Reynolds stress correlations for the cylinder consist of small-scale clusters located in the vicinity of the rear surface of the cylinder and large-scale clusters of Reynolds stress correlations located just downstream of the small-scale clusters. But, a large-scale cluster of Reynolds stess correlations only occurs for the sphere. A well-defined Reynolds stress patterns due to fluctuations along the shear layers produce a weaker Reynolds stress region very close to the rear surface of the cylinder, which occurs as a result of the entrainment between wake and main flows. Peak values of Reynolds stress correlations increase in the base region and then decay sharply in the wake further downstream. The Reynolds stress correlations $\langle u'v'/U_\infty^2 \rangle$ is zero around the horizontal symmetry axis as a result of the symmetrical flow structure and attains its highest magnitude in both sides of the centerline, The measured peak values of Reynolds stresses correlations $\langle u'v'/U_\infty^2 \rangle$ are somewhat higher for the cylinder than the sphere. These numerical values for the cylinder and sphere are 0.138 and 0.039, respectively. The reason of the smaller peak value of $\langle u'v'/U_\infty^2 \rangle$ for the sphere is that the degree of fluctuations and random flow movements owing to 3-D flow. The rms of vorticity patterns $\langle \omega^*_{\mathrm{rms}} \rangle$ display similar behavior for the two models presented in the last row of Fig. 6. In the wake region, vorticity fluctuations $\langle \omega^*_{\mathrm{rms}} \rangle$ for the sphere demonstrate higher levels along the shear layer.

Fig. 7 displays a comparison of time-averaged critical flow characteristics along the vertical and horizontal dashed lines, indicated in Figs. 4–6, for Re = 5000. The structure of turbulent flow, the size of the wake flow region, the location of singular and double points, the peak values of turbulent quantities such as streamwise Reynolds normal stress $\langle u'u'/U_\infty^2 \rangle$, transverse Reynolds normal stress $\langle v'v'/U_\infty^2 \rangle$, Reynolds stress correlations $\langle u'v'/U_\infty^2 \rangle$ and vorticity $\langle \omega_{rms}/U_\infty \rangle$ vary as a function of the cylinder and sphere geometry.

Fig. 8 shows the contours of the normalized TKE for the two models at Re = 5000. When the flow structures of the cylinder are compared to those of the sphere, the sphere has two maxima of TKE, which are located in shear layers, while a single maximum value of the TKE is evident in the wake region of the cylinder. These results reveal that maximum fluctuating velocity occurs in the region close to the saddle point due to the merging of shear layers for the cylinder case. On the other hand, in the case of the sphere, a high rate of fluctuations happens along the shear layer emanating from the periphery of the sphere. A high rate of entrainment between the free-stream and the wake flow regions is developed, and hence the two peak values of the TKE occur on both side of the sphere symmetry plane. The peak value of the TKE for the sphere has a value of 0.083 at a location of $0.89D_s$ and that for the cylinder is 0.225 at a location of $1.69D_c$.

4. Conclusions

The characteristics of the flow field around the cylinder and sphere are compared. The relationship between flow structures and turbulence quantities are presented in terms of instantaneous and time-averaged flow data for Re = 5000 and 10,000. It is known that the flow structures around the cylinder immersed in a free-stream flow is 2-D, on the other hand, 3-D flow takes place around the sphere for the same flow conditions.

The PIV results of time-averaged turbulent structures are consistent with the visualized flow field showing the onset of shear layer instability. The instantaneous vorticity fields reveal an unsteady wavy structure of the sphere wake. Time-averaged and instantaneous flow data reveal that the structure of the turbulent flow and wake flow region, the location of singular and double points, the peak values of turbulence quantities, such as Reynolds stress correlations, vorticity fluctuations and TKE vary as a function of models' geometry and Reynolds Numbers.

Strouhal numbers for the cylinder and the sphere at Re = 5000 are determined as 0.21 and 0.18, respectively. Strouhal numbers

varied between 0.18 and 0.24 for $2500 \leqslant Re \leqslant 10{,}000$ agree well with the results of Jang and Lee (2008), Suryanarayana and Prabhu (2000) and Sakamoto and Haniu (1990).

The flow patterns have a considerable symmetry about the centerline of the cylinder and sphere as shown by the time-averaged flow data. Contours of the time-averaged streamwise velocity component demonstrate that the stagnation point around the symmetry plane moves further upstream for the higher Reynolds number for both models. The shear layer surrounding the recirculation bubble downstream of the cylinder has a region of intensified velocity fluctuations with higher values of the Reynolds stress correlations. On the other hand, concentrations of small scale vortices are more dominant in the wake of the sphere than that of the cylinder. Another important point is that the peak concentrations of Reynolds stress occur very close to the saddle points for both geometries. The maximum value of TKE occurs close to the saddle point for the case of the cylinder while two maximum values of TKE occur along shear layers for the case of the sphere because of the 3-D flow behavior. The peak values of the turbulent kinetic energy for the sphere are approximately three times smaller than those of cylinder case due to the random velocity fluctuations for Re = 5000. The present results can be helpful for developing and validating numerical predictions as well as for designing purposes.

Acknowledgments

The authors would like to acknowledge the funding of the Scientific and Technological Research Council of Turkey under Contract No: 109R028.The authors acknowledge the financial support of Office of Scientific Research Projects of Cukurova University for funding under Contract No. AAP20025 and Selcuk University's Scientific Research Project Office.

References

Achenbach, E., 1972. Experiments on the flow past spheres at very high Reynolds numbers. J. Fluid Mech. 54, 565–575.
Achenbach, E., 1974. Vortex shedding from spheres. J. Fluid Mech. 62 (2), 209–221.
Akilli, H., Akar, A., Karakus, C., 2004. Flow characteristics of circular cylinders arranged side-by-side in shallow water. Flow Measure. Instrum. 15, 187–197.
Balachandar, S., Mittal, R., Najjar, F.M., 1997. Properties of the mean recirculation region in the wakes of two-dimensional bluff bodies. J. Fluid Mech. 351, 167–199.
Bearman, P.W., 2011. Circular cylinder wakes and vortex-induced vibrations. J. Fluids Struct. 27, 648–658.
Bloor, M.G., Gerrard, J.H., 1966. Measurements of turbulent vortices in a cylinder wake. Proc. R. Soc. London, Ser. A 294, 319–342.
Breuer, M., 1998. Numerical and modeling influences on large eddy simulations for the flow past a circular cylinder. Int. J. Heat Fluid Flow 19, 512–521.
Breuer, M., 2000. A challenging test case for large eddy simulation: high Reynolds number circular cylinder flow. Int. J. Heat Fluid Flow 21, 648–654.
Constantinescu, G.S., Squires, K.D., 2003. LES and DES investigation of turbulent flow over a sphere at Re = 10,000. Flow Turbul. Combust. 70, 267–298.
Gerrard, H., 1965. A disturbance–sensitive Reynolds number range of flow past a circular cylinder. J Fluids Mech. 22, 187.
Hadzic, I., Bakic, V., Peric, M., Sajn, V., Kosel, F., 2002. Experimental and numerical studies of flow around sphere at sub-critical Reynolds number. Eng. Turbul. Model Exp. 5, 667–676.
Jang II, Y., Lee, S.J., 2008. PIV analysis of near-wake behind a sphere at a subcritical Reynolds number. Exp. Fluids 44 (6), 905–914.
Jeon, S., Choi, H., 2010. Suboptimal feedback control of flow over a sphere Int. J. Heat Fluid Flow 31, 208–216.
Johnson, T.A., Patel, V.C., 1999. Flow past a sphere up to a Reynolds number of 300. J. Fluid Mech. 378, 19–70.
Kim, H.J., Durbin, P.A., 1988. Observations of the frequencies in a sphere wake and of drag increase by acoustic excitation. Phys. Fluids 31 (11), 3260–3265.
King, R., 1977. A review of vortex shedding research and its application. Ocean Eng. 4, 141–171.
Kiya, M., Ishikawa, H., Sakamoto, H., 2001. Near-wake instabilities and vortex structures of three-dimensional bluff bodies: a review. J. Wind Eng. Ind. Aerod. 89, 1219–1232.
Leder, A., Geropp, D., 1993. The unsteady flow structure in the wake of the sphere. SPIE 2052, 119–126.
Leweke, T., Provansal, M., Ormie'res, D., Lebescond, R., 1999. Vortex dynamics in the wake of a sphere. Phys. Fluid 11 (9), 12.
Lin, J.-C., Towfighi, J., Rockwell, D., 1995. Instantaneous structure of near-wake of a cylinder: on the effect of Reynolds number. J. Fluids Struct. 9, 409–418.
Mittal, R., 1999. Planar symmetry in the unsteady wake of a sphere. AIAA J. 37, 388–390.
Mittal, R., Najjar, F.M., 1999. Vortex dynamics in the sphere wake. AIAA Paper, pp. 99–3806.
Nakamura, I., 1976. Steady wake behind a sphere. Phys. Fluids 19 (1), 5–8.
Noca, H.G. Park, M. Gharib, 1998. Vortex formation length of a circular cylinder (300 < Re < 4000) using PIV. Proceedings of FEDSM'98, June 21–25, Washington, DC, pp. 1–7.
Norberg, C., 2003. Fluctuating lift on a circular cylinder: review and new measurements. J. Fluids Struct. 17, 57–96.
Ozgoren, M., 2006. Flow structure in the downstream of square and circular cylinders. Flow Measure. Instrum. 17, 225–235.
Ozgoren, M., Sahin, B., Akilli, H., Karakus, C., Yayla, S., Ozturk, A., A. Akar, 2006. Investigation of flow structure around a sphere via PIV. I. Ankara National Aerospace Conference, UHUK 06-028, METU Ankara, September 21–23, Turkey.
Parkinson, G.V., 1974. Mathematical models of flow-induced vibrations. In: Naudascher, E. (Ed.), In Flow Induced Structural Vibrations. Springer, Berlin.
Rajagopalan, S., Antonia, R.A., 2005. Flow around a circular cylinder–structure of the near wake shear layer. Exp. Fluids 38, 393–402.
Sahin, B., Ozturk, N.A., 2009. Behaviour of flow at the junction of cylinder and base plate in deep water. Measurement 42, 225–240.
Sahin, B., Ozturk, N.A., Akilli, H., 2007. Horseshoe vortex system in the vicinity of the vertical cylinder mounted on a flat plate. Flow Measure Instrum. 18, 57–68.
Sakamoto, H., Haniu, H., 1990. A study on vortex shedding from spheres in a uniform flow. J. Fluids Eng. 112, 386–392.
Sarpkaya, T., 2004. A critical review of the intrinsic nature of vortex-induced vibrations. J. Fluids Struct. 19, 389–447.
Suryanarayana, G.K., Prabhu, A., 2000. Effect of natural ventilation on the boundary layer separation and near-wake vortex shedding characteristics of a sphere. Exp. Fluids. 29 (7), 582–591.
Taneda, S., 1978. Visual observations of the flow past a sphere at Reynolds numbers between 10^4 and 10^6. J. Fluid Mech. 85 (1), 187–192.
Werle, H., 1980. ONERA photograph. In: Dyke, V. (Ed.), An Album of Fluid Motion. Parabolic Press, Stanford, pp. 32–35.
Westerweel, J., 1993. Digital Particle Image Velocimetry, Theory and Application. Delft University Press.
Williamson, C.H.K., 1996. Vortex dynamics in the cylinder wake. Ann. Rev. Fluid Mech. 28, 477–539.
Williamson, C.H.K., Govardhan, R., 2004. Vortex-induced vibrations. Annu. Rev. Fluid Mech. 36, 413–455.
Wu, J.S., Faeth, G.M., 1993. Sphere wakes in still surroundings at intermediate Reynolds numbers. AIAA J. 3 (8), 1448–1455.
Yun, G., Kim, D., Choi, H., 2006. Vortical structures behind a sphere at subcritical Reynolds numbers. Phys. Fluids 18, 015102.
Zdravkovich, M.M. 1997. Flow around circular cylinders. 1. Fundamentals. Oxford University Press, Oxford, ISBN 0-19-856396-5.